Flame Spread Over Ultra-thin Solids: Effect of Area Density and Concurrent-Opposed Spread Reversal Phenomenon

Anthony Vetturini, Wohan Cui and Ya-Ting Liao* (ID) *, Department of Mechanical and Aerospace Engineering, Case Western Reserve University, 10900 Euclid Ave. Glennan 619, Cleveland, OH 44106-7222, USA*

Sandra Olson and Paul Ferkul, NASA Glenn Research Center, Cleveland, OH 44135, USA

Abstract. There are no existing experimental studies of flame spread rate trends for ultra-thin solid samples. Previous theory has predicted that for concurrent flame in kinetic regime, the flame spread rate decreases as the sample thickness decreases and there is a critical thickness below which burning is not possible. To test this hypothesis, a series of microgravity experiments of concurrent-flow flame spread over samples of ultra-low area densities are conducted using NASA Glenn Research Center's Zero Gravity Research Facility (the 5.18 s drop tower). The tested samples are cellulose-based materials of various area densities, ranging from 0.2 mg/cm^2 to 13 mg/cm^2, as low as one order of magnitude less than those ever tested before. Each sample is 30 cm long by 5 cm wide and is burned in a low-speed concurrent air flow (5 to 30 cm/s). The results show that the concurrent flame spread rate is proportional to the flow velocity relative to the flame and is inversely proportional to the sample area density. A theoretical formulation, provided in this work, suggests that the flame length has a linear relationship with the relative flow speed and has no direct dependency on the sample area density. The experimental data supports this conclusion. From the images recorded in the experiments, a unique flame base tubular structure directed upstream away from the burnout zone is observed for thin samples. This structure is suspected to be due to flame stretching and localized blowoff caused by the oxidative pyrolysis Stefan flows at the sample burnout. This can be an indication that the chemical time becomes comparable to the flow time of the Stefan flow and the tested samples are approaching the kinetically-limited thickness. For the thinnest tested sample (0.2 mg/cm^2), flames with concurrent and opposed dual natures are observed when the air flow rate is low (< 20 cm/s). At the lowest tested flow rate (5 cm/s), the flame spread rate exceeds the air flow rate and the flame transits to an opposed flame in the concurrent flow. The dual nature and flame transition are presented and discussed. This study provides detailed examination through high-resolution images of the transition between the concurrent to opposed flame spread modes.

---

* Correspondence should be addressed to: ; Ya-Ting Liao, E-mail: yating.liao@case.edu

List of Symbols

D	Species diffusivity
k_g	Gas-phase thermal conductivity
L	Latent heat of a solid fuel
L_f	Flame length
L_p	Pyrolysis length
$\dot{m}'$	Total burning rate of a sample per unit width ($= \rho\tau V_f$)
$\overline{\dot{m}''}$	Average burning rate of a sample $\left(= \frac{\rho\tau V_f}{L_f}\right)$
$\overline{\dot{q}''_c}$	Average conductive heat flux
Re	Reynolds number
Re_x	Local Reynolds number
t	Time after drop
T_f	Flame temperature
T_p	Pyrolysis temperature
V_f	Flame spread rate
V_{rel}	Relative flow velocity (concurrent, dual nature, and concurrent-reversed: $V_{rel} = \lvert V_\infty - V_f \rvert$; opposed: $V_{rel} = V_\infty + V_f$)
V_∞	Forced flow velocity
x	Distance away from the upstream leading edge of a sample
y_f	Cross-stream location (away from sample surface) of a flame
α	Gas-phase thermal diffusivity
$\rho\tau$	Sample area density
v	Kinematic viscosity

1. Introduction

Flame spread is one of the most important characteristics of material flammability as it determines the time for controlling or escaping the fires. Understanding this process will help us assess fire hazards and increase the fire safety in space as well as on the earth. During the flame spread process, a flow (either externally imposed or naturally induced by gravity) is usually present. Depending on the flow direction, the flame spread is traditionally categorized into concurrent or opposed. For concurrent flame spread, the flame spreads in the same direction as the flow. The upstream part of the flame base anchors around the burnout region on the sample surface. The flame tip extends in the flow direction and preheats the downstream fuel sample. For opposed flame spread, the flame spreads against the flow and the flame tail extends downstream past the burned portion of the sample. Only a small upstream leading edge region of the flame provides energy to heat up and pyrolyze the sample. In most scenarios (except in very low-speed flows) [1], the concurrent flames are longer and spread faster than opposed flames. Therefore, in this work, we focus on the perceived more hazardous concurrent-flow flame spread.

Numerous studies have been carried out in the last few decades on concurrent flame spread. The controlling mechanism is the heat transfer from the flame to the solid fuel in the preheat and pyrolysis regions [2–4]. When convection dominates, the external flow velocity has significant effects on both the flame length and the

flame spread rate. For upward flame spread, the buoyancy-induced flow accelerates as the flame grows and entrains increasing volume of fresh air. Most experiments observed a continuously growing process of upward flame spread (e.g., [2, 5]). For concurrent forced flow, experiments and theory predicted that the flame would eventually reach a steady spreading state with a constant flame length (e.g. [1, 4, 6–9]). The steady flame spread rate was shown to be function of forced flow speed [1, 7, 9], ambient pressure [1], oxygen percentage [1, 4, 9], and sample inclination angle [2, 10].

Some research focused on characterizing the extinction limits of the flame spread [9, 11–13] in terms of ambient oxygen percentage and flow speed. The extinction (or the flammability) boundary consists of a low-speed quenching branch and a high-speed blowoff branch. The quenching limit is a condition at which the heat loss becomes comparable to the rate of heat generation. For flame spread over solids, the heat loss can be the radiative loss from the solid surface, the radiative loss from the gaseous flame, or the conductive loss from the flame. The blowoff limit is due to insufficient residence time of the reactants (the residence time is smaller than the reaction time i.e., low Damkohler number). Another area of interest is the formation of flamelets observed for nearly quenched flames in opposed flows [14]. These flamelets increase the flame surface-to-volume ratio and enhance the oxidizer transport to the flame and heat flux to the sample surface [14]. They extend a material's flammability past the flame extinction limit and can be dangerous from a fire-safety perspective.

While previous work provides abundant data and mechanism regarding the flame spread, there has been little experimental research into the limiting factor of the sample thickness on the flame spread. For thermally-thin samples, the current understanding is that the flame spread rate is inversely proportional to the sample thickness [4, 15, 16]. This concept was theorized using a steady state energy balance in the solid preheat region and is true for both concurrent and opposed flow [17]. Di Blasi predicted that, for extremely thin samples (< 0.008 cm for a cellulose-based material), in addition to the thermally thin regime, there exists a kinetic regime where the spread rates increase with the sample thickness [16]. In this kinetically-limited regime, the reduced pyrolysis mass flux (associated with extremely thin samples) will eventually cause material flammability to decrease. Essentially, the sample becomes non-flammable when its thickness is below a critical value. This thickness-associated extinction limit was also predicted numerically by Jiang [15]. However, it has not been found in any known previous experimental work.

One of the purposes of this research is to explore the predicted kinetic regime through concurrent flame spread experiments. Samples tested are with area densities lower than ever tested before. To eliminate the complication caused by buoyant flows, tests are conducted in microgravity condition and the imposed air flow speed is independently controlled. By varying the area densities of the sample, the dependence of the flame spread rate and flame length on the sample area densities are studied. The limiting factor of the sample thickness is investigated.

Another purpose of this work is to examine the transition from a concurrent to an opposed flame shown schematically in Fig. 1. In this work, all samples are
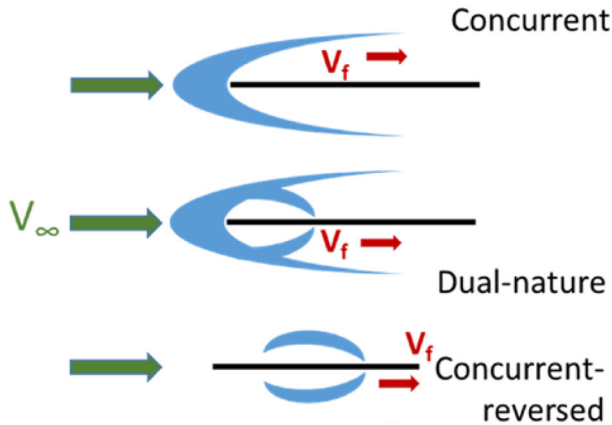
Figure 1. Schematic of the three flame geometries observed in this work.

ignited from the upstream end and concurrent-flow flame spread (Fig. 1 top) is intended. However, flames are observed to exhibit opposed-flow nature near the downstream leading edge (Fig. 1 middle) when the flame spread rate approaches the imposed air flow rate. Similar phenomena were reported by Olson and Miller [1]. In our work, we examine this concurrent-opposed dual nature flame in detail using images captured by high-resolution video cameras. Last, in one of the tests, the flame spread rate exceeds the imposed flow speed. The high-resolution video images clearly demonstrate that the flame switches to an opposed flame mode (in flame fixed coordinate) (Fig. 1 bottom) while spreading in a concurrent flow (in laboratory coordinate). A condition for this transition to happen is discussed in the work.

2. Microgravity Experiment

To accomplish the microgravity flame spread experiments, the NASA Glenn Research Center's Zero Gravity Research Facility (ZGRF) was used (see Fig. 2). The facility provides 5.18 s of microgravity duration. The tests were performed in a low-speed flow tunnel [1] mounted inside of the drop vehicle. The flow tunnel can provide a flow between 0 cm/s and 30 cm/s at various pressure and oxygen conditions. An extremely thin cellulose-based paper (made of mulberry trees) manufactured by Hidakawashi Co. LTD.[1] [18] was identified to test the limiting factor of area density on the flame spread. These thin samples are referred to as TENGU in this work. In addition, cheesecloth fabrics with various area densities were also tested. The area densities of the samples and flow conditions tested in this work are summarized in Tables 1 and 2. For the cellulose density of 1500 mg/

---

[1] Any use of tradenames in this publication is for descriptive purposes only and does not imply endorsement by the U.S. Government.
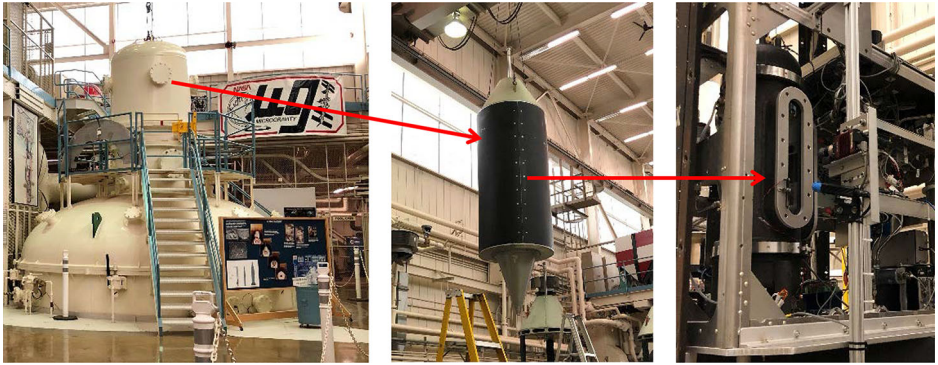
Figure 2. Experiment facility. Left to right: Zero Gravity Research Facility at NASA Glenn Research Center, experiment package, and flow tunnel.
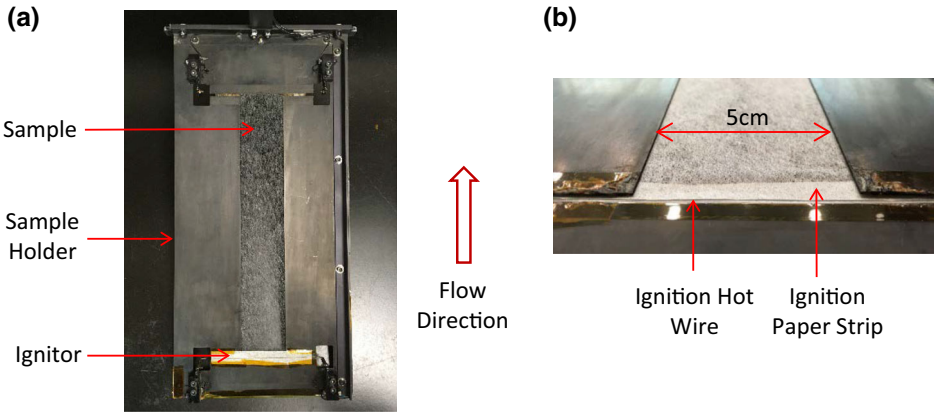

Figure 3. Sample setup. (a) Sample and sample holder. (b) Ignition wire and ignition paper strip.

cm^3, all of the samples except the 13.14 mg/cm^2 cheesecloth are less than the 0.008 cm critical thickness predicted by Di Blasi [16], hence referred to as ultra-thin samples in this work. All tests were performed in 21% oxygen and 1 atm pressure.

The sample setup is shown in Fig. 3. The sample was held in place with Kapton (see footnote 1) tape on a Spring steel sample holder. The sample has a length of 30 cm and an exposed width of 5 cm. A 29-gauge Kanthal (see footnote 1) ignition wire was placed near the upstream edge of the sample, so that the flame would spread in the same direction as the flow after ignition. The wire was straight and under tension to keep good contact with the fabric. For the thinnest (0.2 mg/cm^2) samples, the power of the ignition wire was on at the moment the
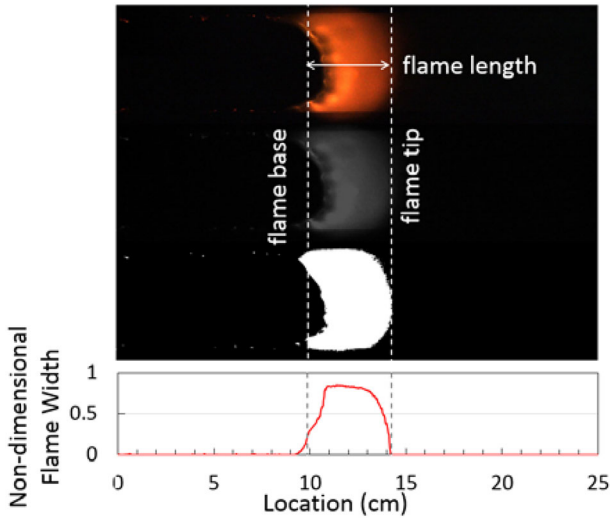
Figure 4.   Image processing and flame location analysis. From top to bottom: raw front-view camera frame, gray-scale image, binary image, non-dimensional flame width versus location.

experiment package was released. For all other tests, the power of the ignition wire was on 0.5 s prior to the drop. The current and the duration of the ignition wire were 3.95 amps and 3 s respectively in all tests. For the thin samples (TENGU), a 1 cm long, 5 cm wide ignition paper strip was placed between the wire and the sample surface (Fig. 3b). The ignition paper strip was made of Kimwipes (see footnote 1) (area density $\sim$ 2 mg/cm^2). The Kimwipes (see footnote 1) ignition strip helped assure ignition of the very thin samples.

The flow velocity for the test was set using a manual pressure regulator that was adjusted for the desired choked flow pressure upstream of a critical flow orifice prior to the test while the gas was flowing. In each test, the pressure upstream of a critical flow orifice was recorded to measure the actual average flow velocity through the test section. These air flow rates are also listed in Table 2 for TENGU samples. Two GigE digital video cameras [Prosilica GT 1920 (see footnote 1)] were used to record the ignition and flame spread processes from the front and side views. The gain and the frame rate of the cameras were set to 18 and 29.97 frames/s respectively. The camera exposure time was auto-adjusted between frames and was recorded on the videos (100 μs to 350 μs for front-view images and 700 μs to 1500 μs for side-view images). A MATLAB (see footnote 1) code was developed to analyze the front-view video images (resolution of front images: 6.52 pixel/mm) and track the flame locations. The procedure (see Fig. 4) includes removing the green LED light, transformation into gray-scale, and transformation into black-and-white binary images. Last, based on the binary images, the non-dimensional flame width (ratio of the white pixels to total pixels across the width of the tracking domain) was calculated. Note that the tracking domain
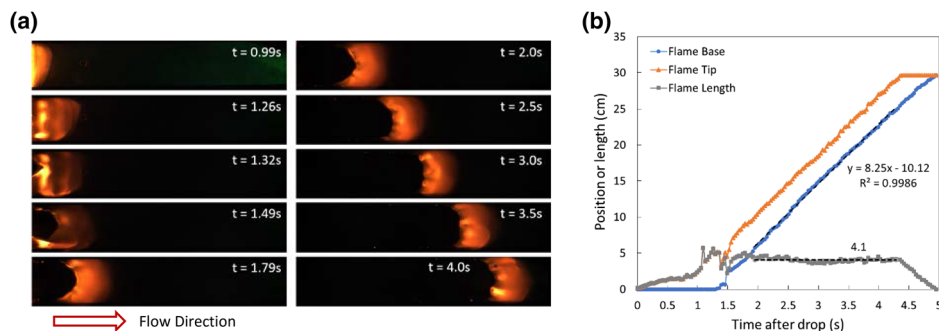
Figure 5. Concurrent flame spread process. Sample area density: 0.5 mg/cm². Air flow speed: 30 cm/s. (a) Front-view video images. (b) Flame tip, flame base, and flame length versus time (uncertainties of the position and time for each data point are ± 0.077 mm and ± 175 μs respectively).

Table 1
Summary of the Sample Thicknesses, Test Conditions, and Test Results for Bleached Cheesecloth Samples

Sample area density ($\rho\tau$: mg/cm²)	Air flow rate (V_∞: cm/s)	Relative flow rate (V_{rel}: cm/s)	Flame spread rate (V_f: cm/s)	Measured flame length (L_f: cm)	Flame nature
13.14	30	29.8	0.20	7.8	Concurrent
4.38	30	28.84	1.16	–[a]	
2	30	27.92	2.08	7.2	

[a]Flame grew beyond the field of view of the camera by the end of the drop test

is slightly wider than the sample width and hence the maximum flame width is below one in Fig. 4. The downstream flame tip and the upstream flame base were defined at non-dimensional flame width at 0 and 0.2 respectively. For the upstream flame base, a non-zero threshold value (0.2) was chosen in order to exclude noises upstream created by smoldering of residue samples along the edges of the sample holder.

Note that in this work, samples were ignited from the upstream end and concurrent-flow flame spread were intended in all tests. However, as the air flow rate decreased, flame spread with different natures (concurrent, dual nature, and concurrent-reversed) were observed (see Table 2). They will be discussed separately in the Sect. 3.

Table 2
Summary of the Sample Thicknesses, Test Conditions, and Test Results for TENGU Samples

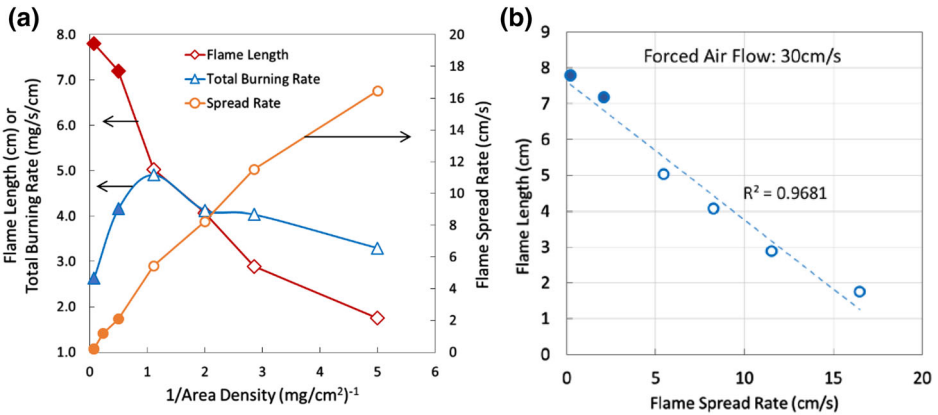| Sample area density ($\rho\tau$: mg/cm^2)	Air flow rate (V_∞: cm/s) (set/actual)	Relative flow rate (V_{rel}: cm/s)	Flame spread rate (V_f: cm/s)	Measured flame length (L_f: cm)	Flame nature
0.90	30/29.7	24.25	5.45	5.0	Concurrent
0.50	30/29.7	21.45	8.25	4.1	
0.35	30/29.2	17.67	11.53	2.9	
0.20	30/31.3	14.82	16.48	1.8	
0.50	15/15.2	11.62	3.58	2.7	Dual nature
0.20	20/19.3	5.96	13.34	2.1	ure
0.20	15/15.0	2.32	12.68	1.8	Concurrent-
0.20	5/4.9	− 7.04	11.94	2.5	reversed

Figure 6. Flame spread rate, flame length, and total burning rate for concurrent flame spread over samples of different area densities in the same forced flow speed (30 cm/s). Open symbols are for TENGU samples and solid symbols are for cheesecloth samples.

3. Results

3.1. Transient Process of Concurrent Flame Spread

Figure 5 shows the front-view images of a representative concurrent flame spread process (0.5 mg/cm^2 sample in 30 cm/s air flow) in this work. The tracked flame tip, flame base, and flame length (the difference between the flame tip and the flame base) versus time are shown in Fig. 5b. Note that t = 0 is defined at the moment the experiment package was released (the onset of the microgravity condition). In the beginning of the test (t < 1 s), the Kimwipes (see footnote 1) igni-

tion paper strip was ignited and the flame tip propagated downstream. In the meantime, flame length grew. At ∼ 1.3 s, the Kimwipes (see footnote 1) strip started to burn out at the upstream edge and the flame base took off. After t = 1.8 s, the flame reached a steady-spreading state, i.e. flame spread downstream steadily with a constant flame length until reaching the end of the sample (30 cm) at t 4.4 s.

It is apparent in Fig. 5b that the flame length had a smooth and monotonic transition to the steady-state flame length. This is different from observed in a previous microgravity experiment, Saffire 1 [7], where a 94 cm-long thin sample was burned in a concurrent flow of 20 cm/s. In Saffire 1, when the flame spread across the first 30 cm of the sample, the flame length first increased but then decreased, resulting in a flame length overshooting before reaching the final flame length at the quasi-steady state. This phenomenon was discussed in a numerical study [8] and attributed to the boundary layer developed upstream to the flame. In Saffire 1, the sample used was a blend of cotton (75% in mass) and inert fiberglass (25% in mass). After the cotton was burned, the fiberglass retained the sample structure, creating a viscous boundary layer upstream to the flame. For small flames that stay close to the sample surface, the flames are sensitive to the flow variation (in both stream and cross-stream direction) inside the boundary layer. For a short sample, the boundary layer is thin and its effect on the flame is minimal [9]. However, for a long sample, when the flame spread downstream along the sample surface, it experiences a decaying flow and the flame length decreases accordingly. In this work, the sample burns away (although there is a solid metal section of the sample holder upstream of the ignition wire). Therefore, we assume the boundary layer development starts at the burnout of the sample. It is reasonable to assume that the flow is fairly uniform and at a constant rate before reaching the upstream burnout point of the sample. This facilitated the observation of the steady state of the flame for the moderate size of the sample in this work.

3.2. Effects of Sample Thickness on Concurrent Flame Spread

3.2.1. Spread Rate, Flame Length, and Total Burning Rate Samples of seven different area densities (see Tables 1, 2) were burned in an approximately same air flow (∼ 30 cm/s). Similar flame development processes leading to a steady spreading state (as described in Sect. 3.1) were observed for all samples except for the 4.38 mg/cm^2 cheesecloth. For the 4.38 mg/cm^2 cheesecloth test, the flame base was observed to spread steadily downstream with a constant spread rate. However, the flame near the tip region did not seem to reach a steady state. The flame length grew throughout the test and did not reach a constant flame length.

The constant flame lengths (if reached) and the spread rates at the steady state with forced air flow ∼ 30 cm/s are compared in Fig. 6. Figure 6a shows that the flame spread rate increases while the flame length decrease as the sample area density decreases. Notice that the flame spread rate over the ultra-thin samples in these tests reached as high as 16.5 cm/s, comparable to the imposed air flow speed. This implies that the flames experienced very different relative flow velocity ($V_{rel} = V_{\infty} - V_f$) in these tests. The effect of the relative air flow velocity will be

discussed in Sect. 3.3. Figure 6b also shows the linear relationship between the flame spread rate and the flame length at the steady state.

For the tested sample thicknesses, Fig. 6a seems to follow classic theory ($V_f \propto 1/\rho\tau$) [4, 15, 16] and does not show any indication that the flame spread rate will decrease with decreasing sample thickness, as Di Blasi [16] has predicted.

For cases where steady spreading state was reached, the total burning rate per unit width can be defined as $\dot{m}' = \rho\tau V_f$. Figure 6a shows that it displays a non-monotonic trend, increasing then decreases as the area density of the TENGU sample decreases. This will be discussed further below.

3.2.2. Flame Shape The flame shapes at the steady spreading state for four different area densities at 30 cm/s forced flow are compared in Fig. 7. Figure 7c shows the overlaid image of the side views of the flames [obtained by extracting the edge of the converted black and white images using Matlab (see footnote 1)]. It shows that the flame shape is more open (the angle between the flame sheet and the sample surface is larger) for a thinner sample. This is suspected to be because the relative velocity is decreasing with decreasing sample thickness, despite a similar absolute air flow rate (~ 30 cm/s) imposed at the tunnel inlet. For a concurrent-flow flame, the combustible pyrolysates need to transport from the sample surface across the flow stream to meet with the fresh air. If the reaction zone and hence the flame shape resemble the flow boundary layer (developed starting at the burnout of the sample, i.e., at $x = 0$), the flame shape can be expressed as: $y_f \sim \frac{4.91x}{\sqrt{Re_x}} \propto \sqrt{\frac{x}{V_{rel}}}$ [19]. Thus, the cross-stream location of the flame (y_f) increases more slowly along the sample surface for a larger relative flow speed, consistent with Fig. 7c. This relative flow rate would also affect the species and thermal diffusion lengths ($\sim \alpha/V_{rel}$ or D/V_{rel}) which in term determine the flame thickness in the cross-stream direction and the flame standoff distance (the distance away from the sample surface) of the flame base. Figure 7c show that the flame in a lower relative flow velocity has a thicker reaction zone. However, the images in Fig. 7c are not able to resolve the flame base standoff distance.

Figure 7d plots the hydrodynamic boundary layers for the four cases. $y_f = \pm\frac{4.91x}{\sqrt{Re_x}}$. The plot resembles the shape of the flames in the side-view images in Fig. 7c.

3.2.3. Special Tubular Flame Sheet Structure One interesting observation from the front-view images (Fig. 7b) is the 'tubes' at the flame base. Inside these tubes, there seems to be a void space (or 'hole') where no combustion occurs. These tubes varied in size and number. However, they were observed throughout the tests as the flame propagated downstream for all tests with sample area densities ≤ 0.5 mg/cm^2. These tubes are generated at the upstream edge of the flame (the flame base) in one image frame and last for a few frames. The exact cause for these tubes is not clear. We propose a possible cause as being due to the Stefan flow 'jet' from the localized strong oxidative pyrolysis in the burnout region on the sample surface. This flow jet can locally stretch the flame base beyond the
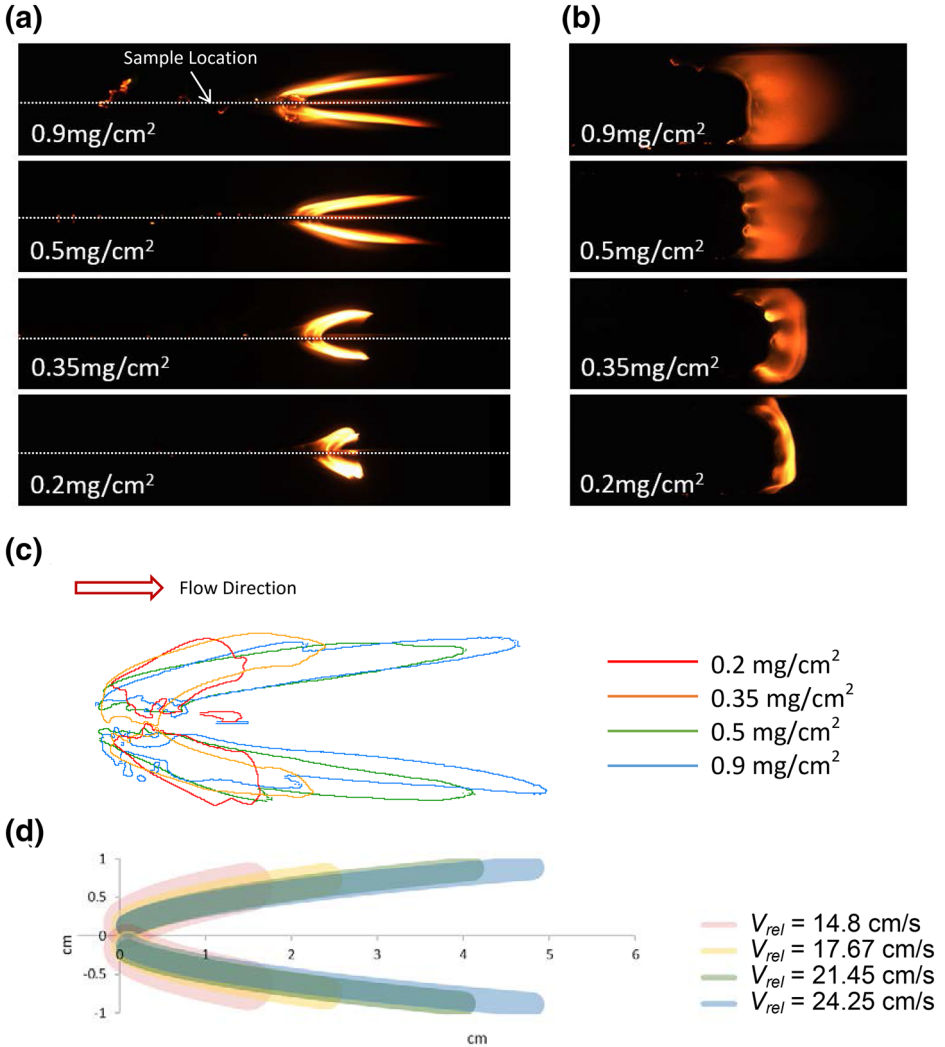
(a)

Sample Location

0.9mg/cm²

0.5mg/cm²

0.35mg/cm²

0.2mg/cm²

(b)

0.9mg/cm²

0.5mg/cm²

0.35mg/cm²

0.2mg/cm²

(c)

Flow Direction

— 0.2 mg/cm²
— 0.35 mg/cm²
— 0.5 mg/cm²
— 0.9 mg/cm²

(d)

V_{rel} = 14.8 cm/s
V_{rel} = 17.67 cm/s
V_{rel} = 21.45 cm/s
V_{rel} = 24.25 cm/s

Figure 7. **Flame shapes for samples of different area densities at a concurrent forced flow speed of 30 cm/s. (a) Side-view video images. (b) Front-view video images (c) Overlay of flame edges deduced from the side-view video images (d) Plotted hydrodynamic boundary layer of the flow:** $y_f = \pm \frac{4.91x}{\sqrt{Re_x}}$ **with Re_x calculated at the relative flow velocity and air kinematic viscosity at room temperature ($\sim$ 300 K) or** $y_f = \pm 2\left(\frac{cm}{s^{1/2}}\right)\sqrt{\frac{x}{V_{rel}}}.$
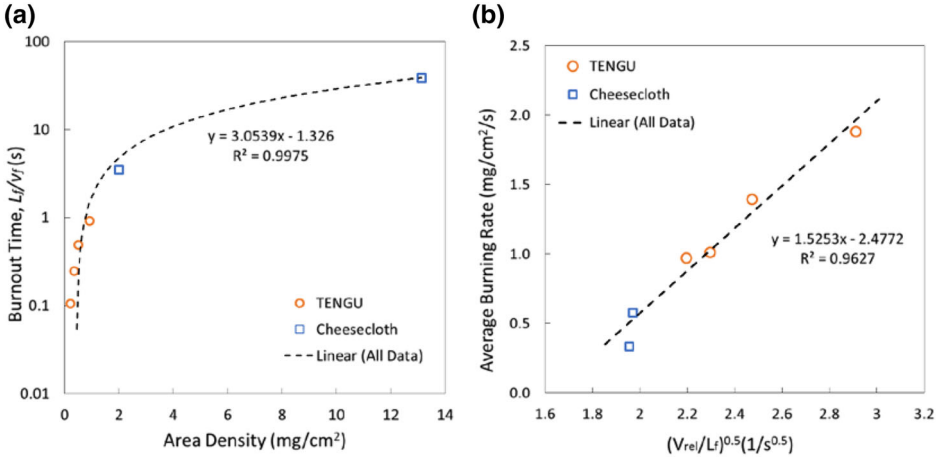
(a)

(b)

Figure 8. **Burnout time and average sample burning rate for different sample thicknesses.**

flammability limit, creating a hole. Similar phenomenon was observed in previous work where PMMA was burned and a vapor bubble ruptured at the molten surface, creating a strong fuel jet that generated a hole in the flame sheet [20]. Assuming the flame temperature and the pressure were similar in all cases, the critical Damkholer number for blowoff is a function of the local stretch rate and the relative oxygen/fuel concentration. As shown in Fig. 6a, the sample total burning rate decreases with the area density for thin samples (≤ 0.9 mg/cm^2). If the fuel concentration locally becomes too low (fuel lean), the reaction rate decreases and the stretch needed to blow off the flame decreases. Theoretically, for a thin enough fuel sample, this stretch due to fuel blowing would extinguish a flame. The observed tubes may be an indication that the samples ≤ 0.5 mg/cm^2 tested were close to this limit.

3.2.4. Burnout Time and Average Sample Burning Rate The burnout time (defined as L_f/v_f, assuming the pyrolysis length is proportional to the flame length) for all concurrent cases are compared in Fig. 8a. It shows that the burnout time increases linearly with the area density (note that the vertical axis is in log scale although the regression is linear due to the data range). However, this does not necessarily mean the average burning rate (area density over burnout time: mass loss per unit time per unit area) is the same in these tests. The average burning rate is defined as:

$$\overline{\dot{m}''} = \frac{\rho\tau}{BurnoutTime} = \frac{\rho\tau v_f}{L_f} \tag{1.}$$

As demonstrated in Fig. 7, the flame shape resembles the flow hydrodynamic boundary layer, i.e., $y_f \sim \frac{x}{\sqrt{Re_x}} \propto \sqrt{\frac{x}{V_{rel}}}$. The average conductive heat flux from the flame to the sample surface in the pyrolysis region can be expressed as:

$$\overline{\dot{q}_c''} \sim \frac{1}{L_p} \int_0^{L_p} k_g \frac{T_f - T_p}{y_f} dx \propto k_g (T_f - T_p) \sqrt{\frac{V_{rel}}{L_p}} \tag{2}$$

where k_g is the thermal conductivity of the gas phase. L_p is the pyrolysis length. T_f and T_p are the flame and the pyrolysis temperatures respectively. If conduction heat flux dominates the heat transfer between the flame and the sample in the pyrolysis region, $\overline{m''}L \sim \overline{\dot{q}_c''}$ and the steady-state pyrolysis length is proportional to the flame length,

$$\overline{\dot{m}''} = \frac{\rho \tau v_f}{L_f} \propto \frac{k_g (T_f - T_p)}{L} \sqrt{\frac{V_{rel}}{L_f}} \tag{3}$$

where L is the latent heat of the solid sample.

In Fig. 8b, the average burning rate (the left hand side of Eq. 3) is plotted against $\sqrt{\frac{V_{rel}}{L_f}}$. It indeed demonstrates a linear relationship. Equation 3 will be used to deduced the flame length below.
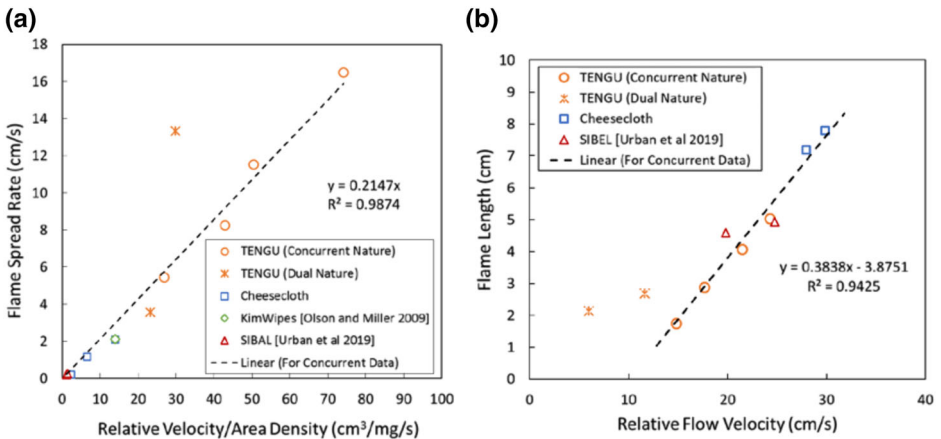

Figure 9. Flame spread rate and flame length for samples with different area densities in different forced flow rates.

3.3. Effects of Relative Flow Velocity on Concurrent Flame Spread

Theory predicts that the flame spread rate is proportional to the relative flow speed [3, 15, 21]. Figure 9 compares all cases of concurrent-flow flame spread obtained in this work and in previous microgravity experiments. These previous data had similar flow conditions (forced flow velocity ~ 30 cm/s, $P \sim 1$ atm, $O_2 \sim 21\%$) and used cellulose-based sample materials, Kimwipes (2 mg/cm^2) [1] and SIBAL fabric (~ 24 mg/cm^2 with 75% cotton and 25% fiberglass) [7, 8]. In Fig. 9a, the spread rates are plotted against $V_{rel}/\rho\tau$. It shows that the flame spread rate can be expressed as follows.

$$V_f \sim \frac{V_{rel}}{\rho\tau} \tag{4}$$

From Eqs. 3 and 4 (assuming T_f and T_p are constant), one can obtain the following.

$$L_f \sim V_{rel} \tag{5}$$

This means that, for the same sample material, the flame length is determined by the relative flow velocity but not directly by the sample area density (for thermally thin samples). In Fig. 9b, flame lengths are plotted against the relative air flow speed. The data supports Eq. 5. Notice that two samples of very different area densities (e.g. thin sample in this work and SIBAL) have similar flame lengths if the relative air flow speeds are close. This was predicted in [15].

Note that in Fig. 9, two tests of TENGU samples in lower forced flow velocities (15 cm/s and 20 cm/s) are also included. The flames in these two tests exhibited concurrent-opposed dual natures and the data did not follow Eqs. 4 and 5. This will be discussed further in the following section.

3.4. Flame Spread with Concurrent-Opposed Dual Nature

When the flow velocity is reduced, flame spread with concurrent-opposed dual nature are observed. In these tests, the flame spread rates were lower than the imposed flow speeds. The flame base encountered a positive flow and remained a concurrent-flow flame. However, in the flame downstream, a leading edge was observed to form and exhibit opposed-flow features. This process is demonstrated using the test of 0.5 mg/cm^2 sample in 15 cm/s air flow as shown in Fig. 10. The front-view image shows that the flame shape was less regular compared with totally concurrent tests at 30 cm/s forced flow. The flame shape also varied between frames. This made the tracking of flame location and flame length challenging. Furthermore, a blue downstream leading edge, typically seen for opposed-flow flame, was observed near the sample surface in both front and side-view images (Fig. 10b). This blue flame edge appeared in the early stage of the flame spread (t ~ 2 s), sometimes bright and sometimes dim, but seemed to be always present until near the end of the test (t ~ 4.5 s).
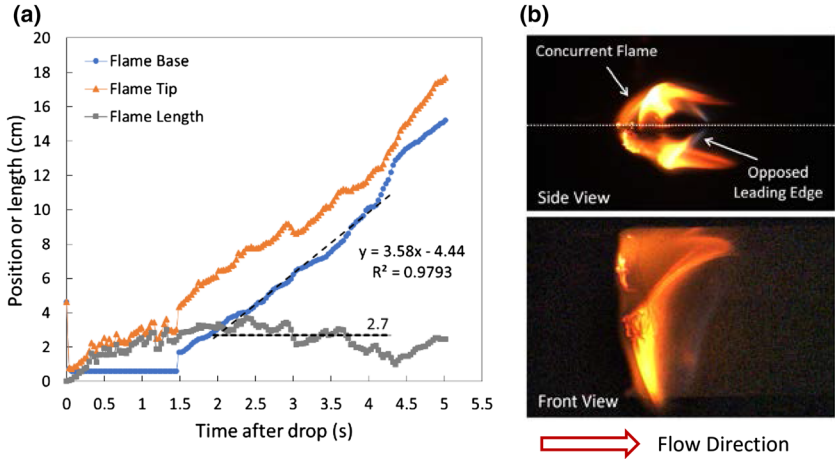
Figure 10. Flame spread with concurrent and opposed-flow dual natures. Sample area density: 0.5 mg/cm². Air flow speed: 15 cm/s. (a) Flame tip, flame base, and flame length versus time (uncertainties of the position and time for each data point are $\pm$ 0.077 mm and $\pm$ 175 μs respectively). (b) Front and side view images of the dual nature flame (t ~ 2.84 s).
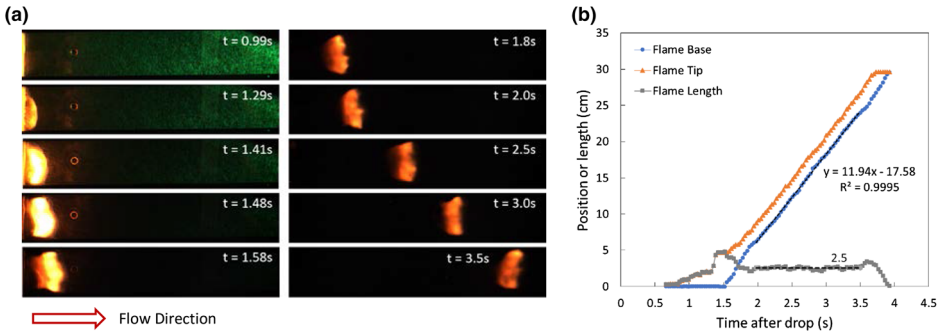

Figure 11. Flame spread with an opposed-flow nature in a concurrent imposed flow. Sample area density: 0.2 mg/cm². Air flow speed: 5 cm/s. (a) Front-view video images. (b) Flame tip (downstream edge), flame base (upstream edge), and flame length versus time (uncertainties of the position and time for each data point are $\pm$ 0.077 mm and $\pm$ 175 μs respectively).

This phenomenon was also observed and reported by Olson and Miller [1]. It was attributed to the flow recirculation downstream of the flame during flow reversals. Olson and Miller hypothesized that the flame, through thermal expansion, acts as a pseudo-solid body and generates steady vortices in the downstream region of the flame in a certain range of Reynolds number (30 to 50 in their cases). In our work, using an estimated flame standoff distance ($\sim$ 0.5 cm) as the characteristic length and the kinematic viscosity of air at 20°C, the Reynolds numbers are $\sim$ 20 and $\sim$ 38 in the two tests where dual nature flames were observed. In this *Re* regime, the flame, if approximated as a cylindrical object, would result in steady recirculation cells (bound vortices) behind it [22]. This flow recirculation could also cause the unsteady irregular flame shape observed in Fig. 10. In the tests where complete concurrent flames were observed, the Reynolds numbers are $\sim$ 49 to 80. For flow over cylinder object, the recirculation cells would become unstable and be washed downstream by the flow [22]. We did not observe flow reversal near the flame tip area.

The flame spread rate and flame length data of the dual nature flames are included in Fig. 9. Generally speaking, the dual nature of the flame seems to strengthen the flame (higher spread rate and longer flame length). It is reasonable since the reversed flow near the downstream edge of the flame brings in more oxygen to the reaction zone, intensifying the reaction. The opposed-flow features near the flame downstream leading edge also brings the flame closer to the sample surface, enhancing the convective heat transfer to the sample fuel.

3.5. Concurrent-Reversed Flame

When the thinnest sample (0.2 mg/cm^2) was burned in 5 cm/s air flow, the flame spread rate ($\sim$ 11.9 cm/s) is higher than the imposed air flow, implying that the flame actually experienced an opposed flow. A flame with an opposed-flow nature (referred to here as a concurrent-reversed flame) was observed throughout the burning process. This process is demonstrated by the front and side-view images in Figs. 11a and 12 respectively. The flame position versus time is plotted in Fig. 11b. Similar to previous tests (Fig. 5), a concurrent flame was first observed at the Kimwipes (see footnote 1) ignition strip (Fig. 12a). After the thin sample was ignited (t $\sim$ 1.3 s), the downstream flame edge took off along the thin sample with a rate that was higher than the imposed air flow speed. Figure 12b shows that the downstream flame edge stayed close to the surface of the thin sample, suggesting a nature of an opposed-flow flame. After the ignition strip burned out (t $\sim$ 1.4 s), the flame upstream edge took off, and the flame length gradually decreased to a constant value. Last (t $>$ 1.8 s), the concurrent-reversed flame spread steadily to the end of the sample (at 30 cm).

Similar to the concurrent flame spread tests (Fig. 7b), the concurrent-reversed flame shows tubular flame sheet structure. However, as shown in Fig. 11a, the tubes were initiated at the downstream edge of the flame, where pyrolysis occurs for an opposed-flow flame. This supports the hypothesis that the tubes were caused by the Stefan flow from the localized oxidative pyrolysis on the sample surface.
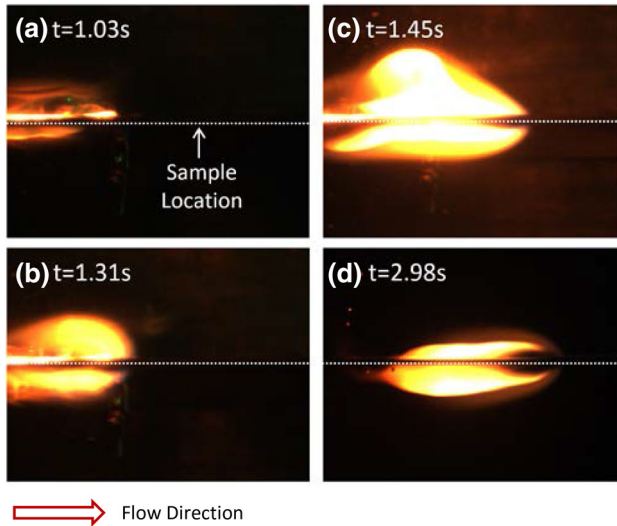
Figure 12. Side-view image of concurrent-reversed flame with the opposed-flow nature. Sample area density: 0.2 mg/cm². Air flow speed: 5 cm/s.

The concurrent-reversed flame was also observed in the test for the 0.2 mg/cm² sample in 15 cm/s air flow. In this test, the flame spread rate (12.68 cm/s) was lower than the imposed air flow (15 cm/s) and the concurrent-reversed flame was not expected. For laminar forced flow over a flat plate, the Blasius solution [19] predicts that the boundary layer thickness at 1.8 cm (flame length in this test) downstream a plate is ~ 0.67 cm (with *Re* evaluated at 20°C), comparable to the flame height observed in the experiment. The flame downstream leading edge was therefore expected to experience a reduced flow in the boundary layer. It is likely that the local flow near the downstream flame edge was reduced to a magnitude comparable to the oxygen diffusion velocity (~ 1 cm/s) or actually even lower than the flame spread rate. Either scenario could trigger the flame nature reversal and result in a concurrent-reversed flame.

For opposed flow flame spread over thin samples, early theory of de Ris predicted that the spread rate is independent of the air flow speed for infinite kinetics [23]. Experimental study of Olson [12] showed that in the finite-kinetics regime, the spread rate has a non-monotonic trend when the air flow velocity increases. The flame spread rate first increases with increased relative air velocity. This was attributed to the greater heat and/or mass transport as the flame is pressed closer to the fuel surface due to thinning boundary layers and enhanced mixing of fuel and oxidizer. After reaching a maximum value, the flame spread rate decreases when the air velocity increases. This was attributed to the Damkohler number effects where the shorter residence times for chemical reaction to occur limit the flame spread process. Eventually a blowoff extinction occurs. Recent microgravity experiments conducted aboard the International Space Station also showed this
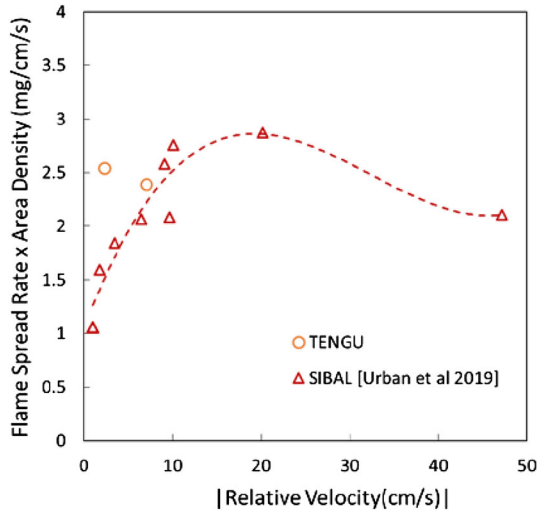
Figure 13. Flame spread rate of opposed flame spread for different relative flow velocities.

dependency [7]. Figure 13 compares the two concurrent-reversed data obtained in this work with the previous opposed-flow microgravity data [7]. In Fig. 13, flame spread rate multiplied by area density is plotted against the magnitude of the relative flow velocity. In the previous opposed-flow flame spread experiments [7], the flow and the flame were in opposite directions. The relative flow velocity is $V_{rel} = V_\infty + V_f$. For the concurrent-reversed flame in this work, the flame traveled in the same direction of the flow. The magnitude of the relative flow velocity is $|V_{rel}| = |V_f - V_\infty|$. For 0.2 mg/cm^2 sample in 5 cm/s air flow, the data overlaps with previous data. However the data for 0.2 mg/cm^2 sample in 15 cm/s departs from the trend line.

In a previous study of Prasad et al. [24], transition of flame spread mode (concurrent vs. opposed) was investigated through both numerical and experimental work. A thermally-thin cellulose-based sample ($\sim$ 6 mg/cm^2) was ignited in the middle of the sample in microgravity and enhanced oxygen condition (35%). In low flow velocities ($\sim$ 5 cm/s), only opposed-flow flame occurred. The flame traveled upstream and created an oxygen shadow in the downstream region, leaving the downstream sample unburned. When the flow is high enough ($\sim$ 20 cm/s), both concurrent and opposed flames were observed, spreading along and against the flow respectively away from the ignition region. In our study, a concurrent flame transits (or flips) to a concurrent-reversed flame. The opposed-nature flame actually traveled in the same direction of the flow (instead of against the flow). This is different from what was observed in Prasad et al. [24].

The flame transition process observed in this work is summarized in Fig. 14. From left to right, the flame transits from concurrent (Fig. 14a), to concurrent-opposed dual-nature (Fig. 14b, c), and then to concurrent-reversed (Fig. 14d, e)
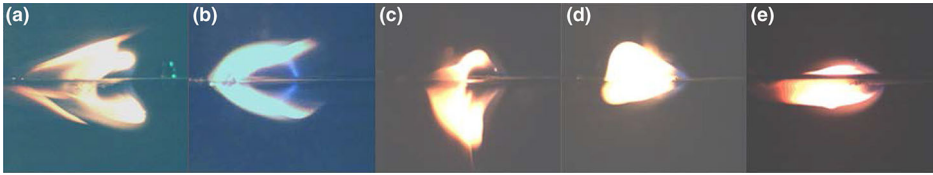
Figure 14. Transition from concurrent, to concurrent-opposed dual nature, to concurrent-reversed flame spread. Test conditions (area density, air flow velocity): (a) 0.2 mg/cm^2, 30 cm/s; (b) 0.5 mg/cm^2, 15 cm/s; (c) 0.2 mg/cm^2, 19 cm/s; (d) 0.2 mg/cm^2, 15 cm/s and (e) 0.2 mg/cm^2, 5 cm/s.

modes. The images were from the last five tests in Table 2 and were greatly enhanced to facilitate the observation of the downstream dim blue tip. Note that for the 'concurrent' flame in Fig. 14a, there seems to be very faint blue flame near the downstream tip. However, the blue tip has a concave curvature rather than the convex curvature expected of an opposed leading edge. In Fig. 14b, c, the blue tip opposed flame leading edge was well-developed and clear. The opposed flame leading edge was hypothesized to be caused by the flow reversal after the flame in a certain range of the Reynolds number (4 to 40 for a long cylinder), as discussed in Sect. 3.4. In Fig. 14d, e, the relative flow speed was further reduced to be comparable to the oxygen diffusion velocity or lower than the flame spread rate, flame fully transits or 'flips' to a concurrent-opposed flame. For thicker samples tested in previous microgravity experiments, the flame quenched before the air flow was further reduced. Concurrent-reversed flame was never observed.

4. Conclusion

A series of microgravity experiments were conducted to study the effects of sample thickness on concurrent-flow flame spread over samples of ultra-low area densities. The sample area densities considered in this work ranged from 0.2 mg/cm^2 to 13 mg/cm^2, as low as one order of magnitude less than ever tested before. The samples were burned in low-speed air flow at 5 cm/s to 30 cm/s. Three types of flame spread were observed, concurrent, concurrent-opposed dual-nature, and concurrent-reversed opposed flame spread.

For concurrent flame spread, the flame spread rate is proportional to the relative flow velocity (forced flow rate minus flame spread rate) and is inversely proportional to the area density of the sample. The flame length has a linear relationship with the relative flow velocity and the sample thickness does not have a direct effect on the flame length.

For dual nature flame, the concurrent flame was observed to exhibit opposed-flow flame features near the downstream leading edge. This phenomenon was also observed and reported by Olson and Miller [1]. It was attributed to the flow recir-

culation downstream of the flame during flow reversals for a certain range of Reynolds number. The dual nature of the flame seems to strengthen the reaction as the reversed flow near the downstream edge of the flame brings in more oxygen to the reaction zone and the opposed-flow feature near the flame downstream leading edge also brings the flame closer to the sample surface, enhancing the convective heat transfer to the sample fuel. These result in higher spread rates and longer flame lengths compared to pure concurrent flames.

For concurrent-reversed flame, the flame had an opposed-flow nature even when it traveled in the same direction as the imposed flow. For this condition to occur, the relative flow rate needs to be reduced to oxygen diffusion velocity or lower than the flame spread rate. For previously tested thicker samples, flame quenched before this condition occurred.

Using the tested samples of ultra-low area densities, a new tubular flame sheet structure was observed at the upstream flame base for concurrent flames or at the downstream leading edge for the reversed flame with opposed nature. This structure is hypothesized to be caused by the strong Stefan flow from the oxidative pyrolysis, stretching the flame and causing localized extinction. The observation of this flame structure may be an indication that the sample thicknesses considered in this study approach the quenching thickness predicted by previous theory [15, 16].

Acknowledgements

References

1. Olson SL, Miller FJ (2009) Experimental comparison of opposed and concurrent flame spread in a forced convective microgravity environment. Proc Combust Inst 32(2):2445–2452
2. Markstein GH, de Ris J (1973) Upward fire spread over textiles. Proc Combust Inst 14(1):1085–1097
3. Fernandez-Pello AC (1979) Flame spread in a forward forced flow. Combust Flame 36:63–78
4. Loh HT, Fernandez-Pello AC (1986) Flow assisted flame spread over thermally thin fuels. Fire Safety Science 1:65–74
5. Saito K, Quintiere JG, Williams FA (1986) Upward turbulent flame spread. Fire Safety Science 1:75–86
6. Tseng Y-T, T'ien JS (2010) Limiting length, steady spread, and nongrowing flames in concurrent flow over solids. J Heat Transf 132(9):091201-1–091201-9

7. Urban DL, Ferkul P, Olson S, Ruff GA, Easton J, T'ien JS, Liao Y-TT, Li C, Fernandez-Pello C, Torero JL, Legros G, Eigenbrod C, Smirnov N, Fujita O, Rouvreau S, Toth B, Jomaas G (2019) Flame spread: effects of microgravity and scale. Combust Flame 199:168–182
8. Li C, Liao Y-TT, T'ien JS, Urban DL, Ferkul DL, Olson S, Ruff GA, Easton J (2019) Transient flame growth and spread processes over a large solid fabric in concurrent low-speed flows in microgravity—model versus experiment. Proc Combust Inst 37(3):4163–4171
9. Zhao X, Liao Y-TT, Johnston MC, T'ien JS, Ferkul PV, Olson SL (2017) Concurrent flame growth, spread, and quenching over composite fabric samples in low speed purely forced flow in microgravity. Proc Combust Inst 36(2):2971–2978
10. Gollner MJ, Huang X, Cobian J, Rangwala AS, Williams FA (2013) Experimental study of upward flame spread of an inclined fuel surface. Proc Combust Inst 34(2):2531–2538
11. Olson SL, Ferkul PV, T'ien JS (1989) Near-limit flame spread over a thin solid fuel in microgravity. Symp (Int) Combust 22(1):1213–1222
12. Olson SL (1991) Mechanisms of microgravity flame spread over a thin solid fuel: oxygen and opposed flow effects. Combust Sci Technol 76:233–249
13. Sacksteder KR, T'ien JS (1994) Buoyant downward diffusion flame spread and extinction in partial-gravity accelerations. Symp (Int) Combust 25(1):1685–1692
14. Olson SL, Miller FJ, Jahangirian S, Wichman I (2009) Flame spread over thin fuels in actual and simulated microgravity conditions. Combust Flame 156(6):1214–1226
15. Jiang C-B (1995) A model of flame spread over a thin solid in concurrent flow with flame radiation. Ph.D. Dissertation, Case Western Reserve University, Cleveland, OH
16. Di Blasi C (1995) Influences of sample thickness on the early transient stages of concurrent flame spread and solid burning. Fire Saf J 25(4):287–304
17. Quintiere JG (2006) Fundamental of fire phenomena. Wiley, West Sussex
18. Hidaka Washi. http://japanese-paper.hidakawashi.com/paper-TENGU/index.html. Accessed 5 Oct 2018
19. White FM (2003) Fluid mechanics. McGraw-Hill, New York
20. Olson SL, T'ien JS (2000) Buoyant low-stretch diffusion flames beneath cylindrical PMMA samples. Combust Flame 121(3):439–452
21. Ferkul PV, T'ien JS (1994) A model of low-speed concurrent flow flame spread over a thin fuel. Combust Sci Technol 99:345–370
22. Kundu PK, Cohen IM (2004) Fluid mechanics, 3rd edn. Elsevier Academic Press, San Diego
23. de Ris JN (1969) Spread of a laminar diffusion flame. Symp (Int) Combust 12(1):241–252
24. Prasad K, Nakamura Y, Olson SL, Fujita O, Nishizawa K, Ito K, Kashiwagi T (2002) Effect of wind velocity on flame spread in microgravity. Proc Combust Inst 29:2553–2560